Light localization in photonic band gaps of quasiperiodic dielectric structures

Kang Wang*
Laboratoire de Physique des Solides, UMR CNRS/Université Paris-Sud, 91405 Orsay, France
(Received 10 May 2010; revised manuscript received 1 July 2010; published 23 July 2010)

Localized light wave states in the photonic band gaps in two-dimensional octagonal and decagonal quasiperiodic dielectric media are investigated by considering the corresponding approximant structures. The structure effects on the local resonances at high-symmetry centers are studied in terms of the interscatterer correlation and the coupling strength between neighbor scatterers is analyzed as a function of the local symmetry order, the structure dielectric contrast, and the scatterer size. It is shown that an interscatterer distance threshold can be defined for the light localization regime. The threshold is determined by the geometrical and dielectric properties of the scatterers and independent of the local symmetry. It is thus likely a universal parameter for light localization in dielectric structures containing high-symmetry centers.

DOI: 10.1103/PhysRevB.82.045119 PACS number(s): 42.25.Bs, 61.44.Br

I. INTRODUCTION

Light exhibits different behaviors depending on the medium through which it propagates. It is classically known that light waves are localized in the sense of Anderson, subject to destructive interferences, in disordered strongly scattering dielectric structures.[1–4] Such structures can lead, besides, to photonic band-gap opening.[5] In perfectly ordered dielectric structures, such as simple periodic photonic structures, light waves are described by extended Bloch states, and photonic band gaps can be obtained as well.[6] Quasiperiodic (QP) structures, being nonperiodic but yet deterministic,[7] differ fundamentally from the above structures. Following the pioneer works of Refs 5 and 6 on random and simple periodic structures, much interest has been aroused on various QP structures in dielectric materials. Concerning light propagation in one-dimensional (1D) QP dielectric structures, attentions are mainly focused on the lack of periodicity and the structure self-similarity, and photonic band-gap opening and light localization are shown to occur in such structures.[8,9] Higher dimensional QP structures differ from the 1D ones, as well as from the simple periodic and random ones, by their high degree rotational symmetries. In the two-dimensional case, QP structures are characterized by octagonal, decagonal, or dodecagonal rotational symmetries and such dielectric structures display many particular features. It has been shown that an octagonal dielectric structure exhibits flat frequency bands and near isotropic band gaps in all the directions of the space,[10] that have potential applications on photonics. These structures present also fundamental interests, such as relations between photonic band gaps and the QP structure order, as well as structure effects on the light wave states at different structure scales. The latter issues are raised, in particular, by the report that light localization occurs in the dodecagonal structure.[11] As a matter of fact, many studies on these structures have been conducted, concerning, noticeably, photonic band-gap properties,[10,12–19] light localization in octagonal,[20] decagonal,[18] and dodecagonal[11,21] structures, defect-related localization and transmission,[22,23] laser effect,[24,25] as well as light emission.[26,27] Indeed, these complex structures provide instructive examples for investigating light wave behaviors in complex dielectric media, in relation with structure environments at various scales, especially the effects of global order and local configurations on photonic gap opening and light localization. As far as the latter is concerned, we have shown that, differently from the conclusion of Ref. 11, light localization occurs in octagonal and decagonal QP dielectric structures at high-symmetry local centers.[18,20] Such localization effect is due to local resonance between neighbor scatterers in Mie resonant mode, favored by high degree rotational symmetries. Moreover, unlike the classical cases, introduction of structure disorder leads to dislocalization effect.[20]

In this work we investigate the localized light wave states in the octagonal and the decagonal dielectric structures, and, in particular, the correlation between scatterers in Mie resonant mode, in order to understand the consequence of the geometrical and dielectric parameters on the localization effect. The comparison between the octagonal and the decagonal structures will further allow us to probe the effects of the local structure order on the light wave states in these complex media, especially in the localization regime, and to determine the fundamental parameters that govern the interscatterer resonance.

II. RESONANCE AT HIGH-SYMMETRY CENTERS

As compared to periodic structures, QP dielectric structures display higher rotational symmetry orders, thus favoring the formation of resonant states on local structure patterns displaying the maximum rotational symmetry of the quasilattice. As a matter of fact, such local centers correspond, for the octagonal and decagonal quasilattices, to octagonal and decagonal rings formed by equidistant dielectric scatterers. In a nearest-neighbor approximation, the frequency levels of all the resonant states formed on these rings can easily be calculated.[18,20] The coupling between neighbor scatterers can be expressed by a coupling parameter g that has units of frequency

$$g \propto -\int d\vec{\rho}\phi^*(\vec{\rho})H\phi(\vec{\rho}-\vec{R}), \tag{1}$$

where $\phi(\vec{\rho})$ is the wave function on an individual scatterer, R the interscatterer distance on the ring, and H the Hamil-

tonian. The eigenfrequency for an individual scatterer, $\bar{\omega}_0$, is just the Mie resonance frequency.[18,20] Using the Hükel theory,[28] we obtain, for weak coupling, the eigenfrequency levels for the resonant states on the octagonal ring

$$\bar{\omega} = \bar{\omega}_0 - g, \quad \bar{\omega}_0 - \frac{g}{\sqrt{2}}, \quad \bar{\omega}_0, \quad \bar{\omega}_0 + \frac{g}{\sqrt{2}}, \quad \bar{\omega}_0 + g. \quad (2)$$

For s waves on the scatterers (the first Mie resonance mode), these resonant states are described, respectively, by the Γ_1, Γ_5, Γ_6, Γ_7, and Γ_3 representations under the D_8 group.

For the decagonal ring, we have

$$\bar{\omega} = \bar{\omega}_0 - g, \quad \bar{\omega}_0 - \frac{\tau}{2}g, \quad \bar{\omega}_0 - \frac{\tau-1}{2}g, \quad \bar{\omega}_0 + \frac{\tau-1}{2}g, \quad (3)$$

$$\bar{\omega}_0 + \frac{\tau}{2}g, \quad \bar{\omega}_0 + g$$

with the golden number $\tau=(1+\sqrt{5})/2$. For s waves on the scatterers, these resonant states are described, respectively, by the Γ_1, Γ_5, Γ_6, Γ_7, Γ_8, and Γ_3 representations under the D_{10} group.

Γ_3 corresponds to the antibonding state for the two rings, with the eigenfrequency level given by

$$\bar{\omega}_{\Gamma_3} = \bar{\omega}_0 + g. \quad (4)$$

The eigenfrequency $\bar{\omega}_{\Gamma_3}$ of the antibonding state provides thus direct information on the coupling strength between neighbor scatterers on the rings.

III. APPROXIMANT STRUCTURES

The octagonal and decagonal quasilattices exhibit, respectively, global average eightfold and tenfold rotational symmetries, and long-range octagonal and decagonal bond-orientational symmetries. We will consider here their respective approximant structures that are periodic, thus allowing exact resolution of Maxwell's equations. These structures are also good candidates for studying local scale effects since they locally reproduce the parent quasiperiodic structure patterns. The two approximant lattices studied here are shown in Fig. 1.

These approximants are both formed by tiles with edge length a. The octagonal approximant is constructed by squares and rhombi with $\pi/2$ inner angle. It displays a square unit cell containing 41 nodes, with a cell size of $a(3+2\sqrt{2})$ and a node density of 1.21. The decagonal approximant is constructed by $2\pi/5$ and $\pi/5$ rhombi. It displays a unit cell in the form of $2\pi/5$ rhombus which contains 76 nodes. The unit cell is characterized by a width of $a\sqrt{5}\tau^3$ and a height of $a\sqrt{5}\tau^5/\sqrt{1+\tau^2}$, with a node density of 1.23. These two structure can be described, respectively, as the 3/2 approximant of the octagonal QP lattice and the (8/5,13/8) approximant of the decagonal QP lattice in a cut-and-projection description. As a matter of fact, these two structures can be obtained, respectively, by approximating $\sqrt{2}$ with 3/2 in the octagonal QP lattice, and τ with 8/5 and 13/8 along, respectively, the x and y axes in the decagonal QP lattice, in the formalism of Refs. 29 and 30.

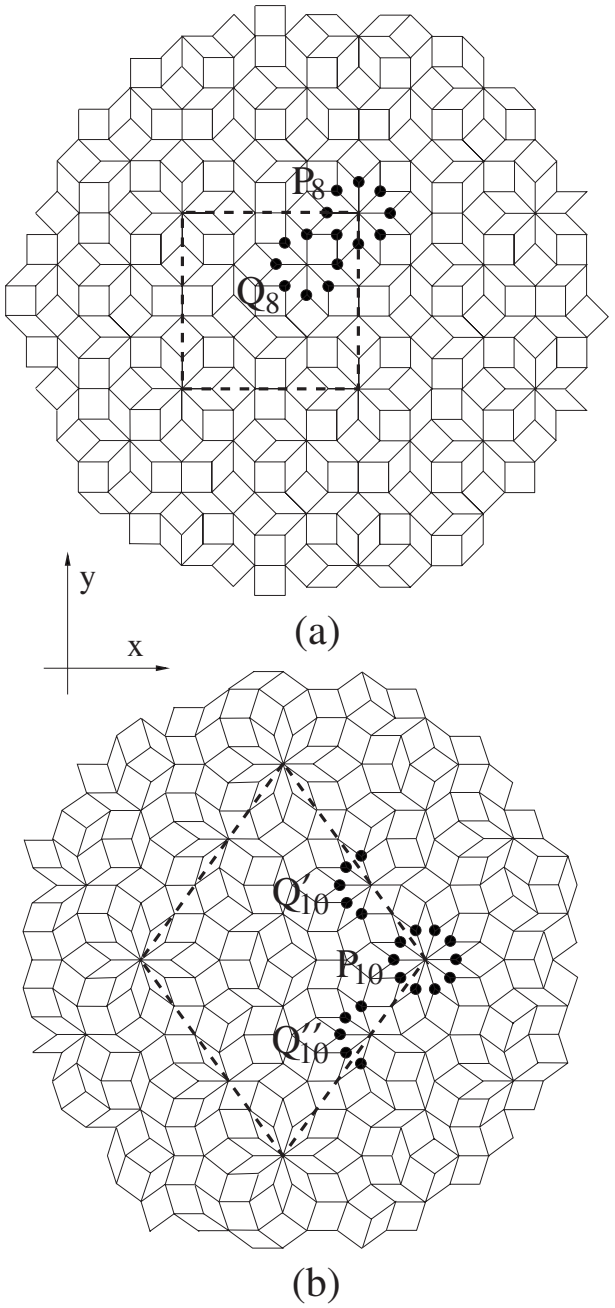

FIG. 1. [(a)] The octagonal and [(b)] the decagonal approximant lattices investigated in the present work. The unit cells are delimitated by dashed lines. The two approximants contain, respectively, octagonal (P_8) and decagonal (P_{10}) rings, as well as incomplete rings (Q_8, Q'_{10}, and Q''_{10}).

These two approximant structures display global average pseudoeightfold and pseudotenfold rotational symmetries and octagonal and decagonal bond-orientational symmetries. They contain, respectively, eightfold and tenfold local centers (patterns P_8 and P_{10} in Fig. 1) that are maximum symmetry centers for their respective parent QP lattices.

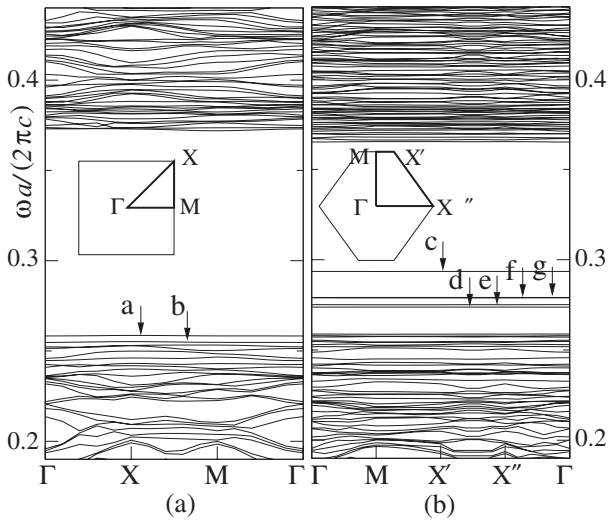

FIG. 2. Band diagrams in the vicinity of the lowest photonic band gaps for [(a)] the octagonal [(b)] the decagonal approximant dielectric structures with scatterer radius $r=0.25a$ and dielectric constant $\epsilon=12$. Localized states inside the band gaps are labeled from a to g.

IV. LOCALIZATION IN THE BAND GAPS

A. Band structures

The approximant dielectric structures are formed by scatterers that are infinite high dielectric cylinders placed perpendicular to the lattice plane at the lattice nodes in a vacuum background. In order to illustrate the relation between the resonant states and the photonic band structures, as well as their dependence on the dielectric and geometrical parameters, we first discuss in detail the case of scatterers of dielectric constant $\epsilon=12$ and radius $r=0.25a$. This configuration leads to a filling rate of about 23.7% and 24.2% and an average dielectric constant $\bar{\epsilon}$ of about 3.61 and 3.66 for, respectively, the octagonal and decagonal structures.

Maxwell's equations are solved for TM polarization using a plane-wave method. Well-defined photonic band gaps are obtained. For simplicity we will limit the investigation to the first (lowest) photonic band gaps and the inside light wave states. Figure 2 displays a portion of the band diagrams around the first photonic band gaps for these two structures.

Several flat bands, indicated by arrows and labeled from a to g, are found inside the band gaps. These bands correspond to localized states that are confined on particular local structure patterns, as shown by the corresponding spatial electric field distributions in Fig. 3, where the field patterns are lettered following the band labeling in Fig. 2. As shown in our previous works[18,20] and further discussed below, these states are resulted from resonances at local scales and therefore not involved in the photonic band-gap opening. The identification of these states as local modes allows a better estimation of the gap parameters. We obtain for the two approximant structures almost the same midgap frequency $\bar{\omega}_{gap}\approx 0.31$, and a relative gap width of 38% and 34%, respectively, for the octagonal and decagonal structures.

The fact that these two structures display the same band-gap position is quite natural. The midgap frequency is related

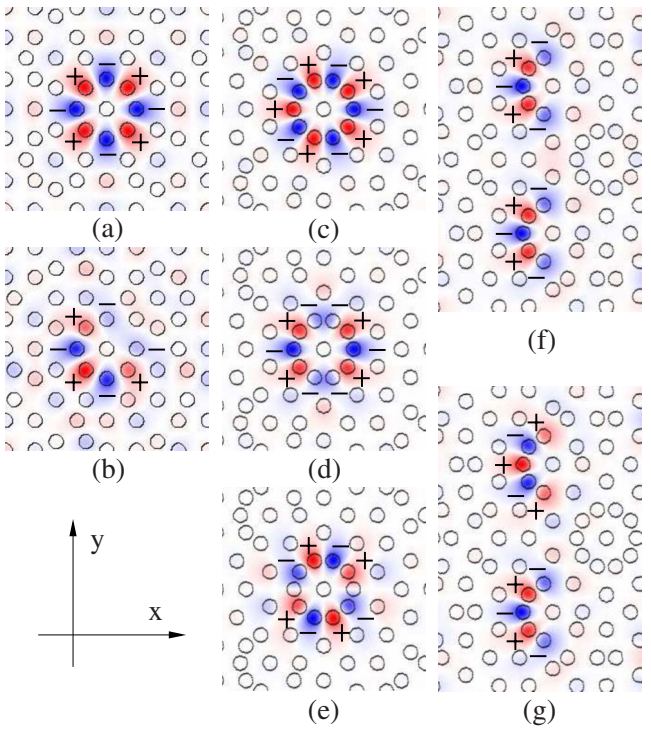

FIG. 3. (Color online) Electric field patterns for the localized states inside the first photonic band gap of [(a) and (b)] the octagonal and [(c) to (g)] the decagonal approximant structures. The patterns are lettered following the band labeling in Fig. 2. The "+" and "–" signs indicate the field polarities.

to a set of reciprocal vectors K_p that are determined by the global structure order, as well as to the average dielectric constant $\bar{\epsilon}$, through the relation

$$\bar{\omega}_{gap} = \pi \frac{cK_p}{\sqrt{\bar{\epsilon}}}. \tag{5}$$

The reciprocal vectors K_p, on which the gaps are opened, have their magnitudes inversely proportional to the average distances between planes passing by the scatterer axes, that have close values for the octagonal[16] and the decagonal structures.[18] The parent QP dielectric structures should display similar gap positions as well since the reciprocal vectors K_p differ little between the QP structures and the approximant ones.[31] Besides, as mentioned above, these two structures have similar average dielectric constants, due to their close node densities. So it is natural that they display similar $\bar{\omega}_{gap}$. More important, as we will see below, the dependence of the gap position on the average dielectric constant will enable us to follow the evolution of the resonant states inside the band gaps, and to investigate the coupling between scatters as functions of the dielectric contrast and filling rate of the structures.

B. Light localization

Now let us consider in more detail the localized states in the photonic band gaps. The corresponding electric field patterns are shown in Fig. 3, where (a) and (b) display the field

patterns corresponding to the two bands close to the low gap edge of the octagonal structure while (c)–(g) depict those corresponding to the five bands inside the gap of the decagonal structure. Indeed, the modes in (a), (c), (d), and (e) are all formed at maximum symmetry local centers, that are octagonal [P_8 in Fig. 1(a)] and decagonal [P_{10} in Fig. 1(b)] rings. The modes in (a) and (c) are described by the Γ_3 representation under the D_8 and D_{10} groups, and correspond to *s*-wave antibonding states. The two modes in (d) and (e), that are orthogonal to each other and can both be described by the Γ_8 representation under D_{10}, correspond to doubly degenerate partially antibonding states (see Sec. II).

We note as well that the two approximants considered here have the particularity of containing both local structure patterns that can be viewed as incomplete rings. There is one such pattern in the octagonal approximant that is an incomplete octagonal ring [pattern Q_8 in Fig. 1(a)] while the decagonal approximant contains two patterns that are incomplete decagonal rings [patterns Q'_{10} and Q''_{10} in Fig. 1(b)]. Resonant states, with more extended field distribution on the scatterers, especially near the broken ends of the incomplete rings, are formed as well on these patterns [Figs. 3(b), 3(f), and 3(g)], with frequency levels lying below the antibonding states for each structure (band *b*, *f*, and *g*, respectively, in Fig. 2).

Let us consider the Γ_3 antibonding states on the octagonal and decagonal rings. These states correspond to the frequency levels $\bar{\omega}_{\Gamma_3} \approx 0.25$ and $0.29(\omega a/2\pi c)$, respectively, for the two rings. For *s* waves, the initial eigenmode on the individual scatterers corresponds to the first Mie resonance,[18,20] that occurs, on an individual infinite cylinder with dielectric constant $\epsilon=12$, for the size parameter $x=2\pi r/\lambda_0 \approx 0.30$,[32] with λ_0 the incident wavelength in the surrounding medium. This corresponds, for $r=0.25a$, to the frequency $\bar{\omega}_{Mie}=\bar{\omega}_0 \approx 0.19(\omega a/2\pi c)$. The coupling parameter *g* values can thus be estimated from Eq. (4). We obtain $g \approx 0.06$ and $0.10(\omega a/2\pi c)$ for, respectively, the octagonal and the decagonal rings.

The localization is induced by interscatterer resonance. It is thus interesting, for a better understanding of the localization mechanism, to investigate the coupling between the scatterers in the localized states. Below we probe the consequences of the geometrical and dielectric parameters that determine the correlation between the scatterers and thus influence the localization. We follow the coupling parameter evolution as a function of both the dielectric constant ϵ and the radius *r* for the scatterers in the two structures. We will show that it is possible to draw a threshold for the localization regime that is determined by ϵ and *r*.

As mentioned above, for a given lattice, the band-gap position (midgap frequency) scales inversely with the square root of the average dielectric constant $\sqrt{\bar{\epsilon}}$ [Eq. (5)]. It is therefore inversely correlated with both the size *r* and the dielectric constant ϵ of the scatterers. The Mie resonance frequency level, on the other hand, is inversely correlated with the square root of the scatterer dielectric constant $\sqrt{\epsilon}$ and scales inversely with the scatter size *r*. So that the localized states inside the band gaps will persist to lower filling rate and dielectric contrast. This will allow us to study the evolution of the coupling parameter *g* for decreasing ϵ and *r* in the dielectric approximant structures.

Several series of structures, constructed on the same octagonal and decagonal approximant lattices of Fig. 1 but with different sizes and dielectric constants for the scatterers, are considered. For simplicity, four of them will be discussed here in detail, other configurations leading to analog results. Two of these series are characterized by the geometrical or dielectric parameters considered above, i.e., one with constant scatterer radius $r=0.25a$ and decreasing dielectric constant ϵ, the other with constant dielectric constant $\epsilon=12$ and decreasing scatterer radius *r*. The other two series are characterized by weaker geometrical and dielectric parameters: one with constant $r=0.18a$ and decreasing ϵ; the other with constant $\epsilon=7$ and decreasing *r*. Maxwell's equations are solved on these structures, and the coupling parameter *g* values are subsequently estimated from Eq. (4). The *g* value variations as a function of *r* and ϵ for these structures are displayed in Figs. 4(a) and 4(c).

Figure 4 shows that *g* is stronger on the decagonal ring than on the octagonal one for the same ϵ and *r*. This is not surprising. Indeed, the Mie state wave function $\phi(\vec{\rho})$ on individual scatterers decays with increasing distance ρ, thus the *g* value is inversely related to the interscatterer distance *R* [Eq. (1)]. As a matter of fact, the interscatterer distance for the decagonal ring ($R_{dec} \approx 0.618a$) is about 20% shorter than that for the octagonal ring ($R_{oct} \approx 0.765a$), the interscatterer coupling is thus stronger on the former. As mentioned in our previous works,[18,20] high local symmetry favors the formation of localized state by favoring the coupling between neighbor scatterers. Here the difference in the coupling parameters between the octagonal and the decagonal rings further illustrates this point. A direct consequence of the local symmetry is the position of the localized state frequency levels in the band gaps. The latter have similar positions and widths for the octagonal and decagonal structures, therefore the stronger coupling between scatterers on the decagonal ring leads to deeper positions for the localized states in the band gap, as shown in Fig. 2.

Moreover, *g* decreases both with decreasing ϵ and *r*. This is natural because, besides the dependence of the Hamiltonian *H* on the dielectric function, a weaker ϵ for the scatterers leads to a weaker magnitude for the wave function $\phi(\vec{\rho})$, and a weaker radius *r* leads to a more restricted spatial distribution for $\phi(\vec{\rho})$. It is therefore not surprising that the coupling parameter *g* decreases following either the dielectric constant or the scatterer radius.

Finally, Fig. 4 shows that the coupling parameter *g* approaches zero for certain *r* and ϵ values, that are, moreover, larger for the octagonal ring than for the decagonal one. As a matter of fact, for constant scatterer size $r=0.25a$, the coupling parameter *g* approaches zero for $\epsilon \approx 4.7$ and 3.9 for, respectively, the octagonal and the decagonal rings; while for a weaker scatterer size $r=0.18a$, *g* approaches zero for $\epsilon \approx 7.5$ and 5.5 for, respectively, the two rings [Fig. 4(a)]. Similarly, for constant dielectric constant $\epsilon=12$, *g* approaches zero for $r \approx 0.14a$ and $0.11a$ for, respectively, the octagonal and decagonal rings while for a weaker dielectric constant $\epsilon=7$, *g* approaches zero for $r \approx 0.19a$ and $0.15a$ for, respectively, the two rings [Fig. 4(c)].

The coupling parameter *g* reflects the strength of interaction between neighbor scatterers. The Mie resonance in-

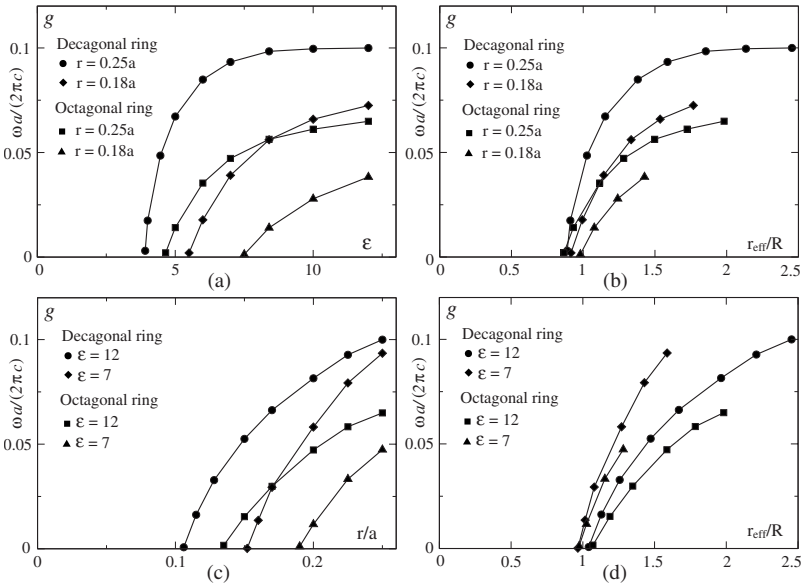

FIG. 4. The coupling parameter g evolutions on the octagonal and the decagonal rings, as a function of [(a)] the scatterer dielectric constant ϵ and [(c)] the scatterer radius r, obtained using Eq. (4). The corresponding g variations plotted as a function of the ratio between the scatterer effective radius r_{eff} and the interscatterer distance R are displayed, respectively, in (b) and (d).

creases the interaction range of a dielectric scatterer with light waves,[32] leading to a correlation region larger than the scatterer size. The correlation region is described by the scattering cross section. A cylindrical scatterer of radius r has a geometrical cross section per unit length of $2r$, for a light wave propagating perpendicularly to its axis. It yields, in Mie resonance mode, a scattering cross section per unit length C_{sca} (Ref. 32) that is larger than $2r$. The cross section increase is usually described by the so-called scattering efficiency $Q_{sca}=C_{sca}/2r$ and an effective radius for the scatterer, r_{eff}, that characterizes the scatterer correlation region, can be defined as

$$r_{eff}=\frac{1}{2}C_{sca}=Q_{sca}r. \tag{6}$$

The effective radius r_{eff} decreases with both ϵ and r. It is therefore instructive to look at the coupling parameter g variation as a function of the scatterer effective radius r_{eff} for the two rings, in relation with their respective interscatterer distance R. For this purpose, the g variations in Figs. 4(a) and 4(c) are replotted, respectively, in (b) and (d), as a function of the ratio between these two lengths, r_{eff}/R, for the first Mie resonance.

Figures 4(b) and 4(d) show that, for both the two rings, g decreases with the effective radius r_{eff} and approaches zero when r_{eff} becomes comparable to R in all the cases ($r=0.25a$ and $0.18a$, and $\epsilon=12$ and 7). For a direct comparison, the effective radius r_{eff} values for $g\sim 0$, as well as the corresponding length ratios r_{eff}/R, are listed in Table I. Indeed, Fig. 4 illustrates clearly the dependence of the interscatterer resonance on the scatterer effective radius. The resonance is significant for large r_{eff}. It decreases with decreasing r_{eff}, before reaching zero when the effective radius approaches the interscatterer distance R.

The light localization is associated with the interscatterer resonance. It is thus interesting to compare the light wave states for scatterer sizes and dielectric constants that lead to r_{eff} well above and below R. As a matter of fact, if we look at the field distributions, we can see that, in the first case, the light waves are predominately localized on the rings while in the second case, extended wave states become non negligible. This is illustrated by Fig. 5, where the electric field magnitudes for bands a and c in Fig. 2, normalized to their

TABLE I. Scatterer radii r, dielectric constants ϵ, effective radii r_{eff}, and r_{eff}/R ratios for the octagonal and decagonal rings for $g\sim 0$. The resonant state frequency levels, the corresponding vacuum half wavelengths, and the optical path lengths between neighbor scatterers are also listed.

	Scatterer radius $r(a)$	Dielectric constant ϵ	Scatterer effective radius $r_{eff}(a)$	r_{eff}/R	Frequency $(\omega a/2\pi c)$	Half wavelength $\frac{1}{2}\lambda_0(a)$	Optical path length $\Delta(a)$
Octagonal ring, $R=0.765a$	0.25	4.7	0.66	0.87	0.39	1.27	1.34
	0.18	7.5	0.75	0.98	0.38	1.33	1.39
	0.14	12	0.82	1.07	0.36	1.39	1.43
	0.19	7	0.75	0.98	0.37	1.33	1.39
Decagonal Ring, $R=0.618a$	0.25	3.9	0.55	0.89	0.48	1.05	1.11
	0.18	5.5	0.57	0.92	0.48	1.05	1.10
	0.11	12	0.64	1.04	0.46	1.10	1.14
	0.15	7	0.60	0.97	0.47	1.07	1.12

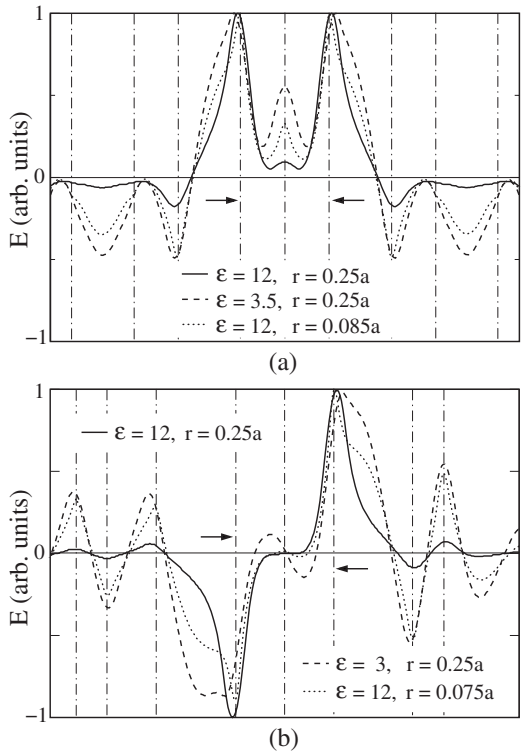

FIG. 5. Normalized electric field distributions for the bands a and c (Fig. 2), in a slice passing through the ring center [(a)] along an axis at $3\pi/4$ for the octagonal approximant structure and [(b)] along an axis at $4\pi/5$ for the decagonal one. The solid lines depict the field distributions corresponding to $r=0.25a$ and $\epsilon=12(r_{eff} \approx 1.52a)$ for the scatterers in both cases. The dashed lines depict that corresponding to [(a)] $\epsilon=3.5(r_{eff}\approx 0.5a)$ and [(b)] $3(r_{eff} \approx 0.4a)$. The dotted lines depict that corresponding to [(a)] $r=0.085a(r_{eff}\approx 0.52a)$ and [(b)] $0.075a(r_{eff}\approx 0.45a)$. The vertical dashed-dotted lines represent the cylindrical scatterer axes and those of the scatterers on the rings are indicated by arrows.

maximum magnitude values, are displayed for several cylinder diameters and dielectric constants, in a slice passing through the ring center in the two structures. It is obvious that, for $\epsilon=12$ and $r=0.25a$, for which $r_{eff}\approx 1.52a$, the field is predominantly concentrated on the scatterers on the two rings, and, for dielectric constants and scatterer sizes for which $r_{eff}<R$ ($r_{eff}\approx 0.5a$ and $0.52a$, and $r_{eff}\approx 0.4a$ and $0.45a$ for the octagonal and the decagonal structures, respectively), the electrical field has significant distribution outside the rings. So, in the later cases, the resonance on the rings is no more the dominant effect and the light wave states can no more be considered as localized on the rings.

This allows us to define a threshold for the localization regime, in terms of the scatterer effective radius in the Mie resonance mode,

$$R \sim r_{eff}. \tag{7}$$

The localization is a dominant effect for interscatterer distances R weaker than r_{eff}. Otherwise the light wave states display extended distributions. The threshold is determined by the scatterer size and dielectric constant, and independent of the ring symmetry.

V. DISCUSSION

The approximant dielectric structures with the resonant light wave states inside the band gaps, provide a unique opportunity for the investigation of the light localization effects on high-symmetry local centers. For both the octagonal and decagonal structures, the coupling between scatterers on such local centers is strong for the distance between scatterers weaker than the scatterer effective radius, $R<r_{eff}$, i.e., when the scatterers are in the correlation region of their neighbors. The correlation length is determined by the geometrical and dielectric parameters of the scatterers, and independent of the ring symmetry. This is not surprising if we consider that the resonance concerns essentially the first neighbor scatterers. It is thus principally determined by the characteristics of the scatterers and the interscatterer distance. The threshold, r_{eff}, can thus be a universal parameter for the light localization in dielectric structures containing high-symmetry centers.

This localization threshold can also be considered in terms of the resonant state wavelength. In fact, for the antibonding states, the field on neighbor scatters have opposite polarities so neighbor scatterers should be separated by a half wavelength $\lambda/2=R$. This can be checked by comparing the half wavelength in vacuum, $\lambda_0/2$, of the resonant states and the optical path length between neighbor scatterers, $\Delta=R+2r(\sqrt{\epsilon}-1)$. The values of $\lambda_0/2$ and Δ are also listed in Table I, together with the resonant state frequency levels. We can see that the relation $\lambda_0/2\approx\Delta$ is verified in all the cases (the slight differences are due to the fact that the field maximum does not coincide exactly with the cylinder axis). Therefore, the ratio r_{eff}/R is equivalent to $2r_{eff}/\lambda$, and the threshold for the localization regime [Eq. (7)] can be expressed in terms of the half wavelength

$$\frac{\lambda}{2} \sim r_{eff}. \tag{8}$$

As far as the coupling parameter g value estimation is concerned, for r and ϵ values leading to a scatterer effective radius r_{eff} well below the interscatterer distance R, Eq. (4) would lead to negative values for g. However, we should keep in mind that, when applying Eq. (4) to the light wave states such as a and c (Fig. 2) inside the band gaps, we are implying that the light waves are essentially confined on the high-symmetry local centers. In fact, as a tight-bonding model, the Hükel theory can only be applied to the high-symmetry local centers when the light waves are concentrated on the rings. For either weak r or weak ϵ leading to $r_{eff}<R$, the light waves display extended distributions. Therefore, the local resonance picture, as well as Eqs. (2)–(4) are no more adequate to describe the light wave states, and an extended wave state model should be used instead. Besides, the slight discrepancies in the effective radius r_{eff} values for $g\sim 0$ in Table I can also be attributed to the weakening of the resonances on the rings, implying surrounding scatterer contributions to g estimation using Eq. (4).

Finally, it is worth discussing further the relation between the approximants and their parent QP structures, in connection with the photonic band-gap opening and the localization effect. As a matter of fact, it is well known that the approxi-

mants and the QP lattices are intimately related, and a rigorous mathematical relation between them can be established. Concerning the band-gap opening, the photonic band structure is determined by the Fourier spectrum of the dielectric structure.[16,18] And the Fourier spectrum of an approximant is related to that of the parent QP structure by a linear shift field, that decreases with increasing approximant order.[29,30,33,34] Therefore, it is possible to draw a direct correspondence relation between the reciprocal vectors on which the band gap is opened for the approximants and those for the parent QP structures.

Indeed, the gap position for an approximant structure is determined, through Eq. (5), by a set reciprocal vectors K_p, that are directly derived, through the shift field, from a set of reciprocal vectors of the parent QP structure.[16,18] The later have their magnitude inversely proportional to the average distance between the scatterer planes, stacked quasiperiodically along the corresponding directions. Pseudo-Brillouin zones can consequently be defined upon these vectors for the octagonal and decagonal QP structures, in the forms of regular octagon and decagon, respectively.[16,18] For reciprocal vectors corresponding to Fourier components of strong intensity, which is precisely the case for these gap vectors, the shifts are very weak.[29,31] Indeed, in the present case, the maximum gap-vector shifts, in magnitude, are about 0.5% and 0.8%, when passing from the QP structures to their respective parent approximants [the 3/2 octagonal and the (8/5, 13/8) decagonal approximants, respectively].[16,18] The differences in node density between these approximants and their respective parent QP lattices being very weak as well (below 0.02%), the QP dielectric structures will display similar band gaps as their respective approximants studied in the present work.

As far as the localization effect is concerned, the light wave resonance occurs on maximum symmetry local centers that are octagonal and decagonal rings, common to both the approximants and their parent QP structures. As a matter of fact, the approximants are of particular interest for the investigation of local structure effects since they locally reproduce their parent QP structures,[35] and thus contain local structure patterns of the later.

Indeed, although the ring structures cannot be reproduced in the lowest-order approximants due to their too small unit-cell sizes,[35] the approximants studied in the present work are of sufficiently high orders to contain each a ring per unit cell. As a matter of fact, they are the lowest-order approximants that can reproduce such ring structures. Higher-order approximants reproduce QP structures on larger scales,[35] with, consequently, more ring structures per unit cell. However, as the resonance effect is resulted from interactions on the ring-size scale, without involving inter-ring interactions,[20] the 3/2 octagonal and the (8/5, 13/8) decagonal approximants constitute the simplest and representative model structures for studying local resonance effect on the maximum symmetry local centers.

VI. CONCLUSION

In summary, light wave states inside the photonic band gaps of the octagonal and decagonal QP dielectric structures, that contain maximum symmetry local centers, are studied comparatively, by investigating the interscatterer correlations on the same local centers in the approximant structures. Structure effects on light wave resonances in and out of the localization regime are analyzed. It is shown that the interscatterer coupling strength varies with the local symmetry, the scatterer size and dielectric constant, and that a threshold for the localization regime can be defined in terms of the relation between the interscatterer distance and the scatterer effective size that determines the correlation range of the scatterers in the Mie resonant mode. Moreover, although the coupling strength varies with the local symmetry order, the localization threshold, being determined by the first neighbor interaction, remains independent of the local symmetry. It can thus be a universal parameter for light localization in dielectric structures containing high-symmetry centers.

*wang@lps.u-psud.fr

[1] P. W. Anderson, Phys. Rev. **109**, 1492 (1958).
[2] S. John, Phys. Rev. Lett. **53**, 2169 (1984).
[3] A. Z. Genack and N. Garcia, Phys. Rev. Lett. **66**, 2064 (1991).
[4] D. S. Wiersma, P. Bartolini, Ad Lagendijk, and R. Righini, Nature **390**, 671 (1997).
[5] S. John, Phys. Rev. Lett. **58**, 2486 (1987).
[6] E. Yablonovitch, Phys. Rev. Lett. **58**, 2059 (1987).
[7] D. Shechtman, I. Blech, D. Gratias, and J. W. Cahn, Phys. Rev. Lett. **53**, 1951 (1984).
[8] W. Gellermann, M. Kohmoto, B. Sutherland, and P. C. Taylor, Phys. Rev. Lett. **72**, 633 (1994).
[9] L. Dal Negro, C. J. Oton, Z. Gaburro, L. Pavesi, P. Johnson, Ad Lagendijk, R. Righini, M. Colocci, and D. S. Wiersma, Phys. Rev. Lett. **90**, 055501 (2003).
[10] Y. S. Chan, C. T. Chan, and Z. Y. Liu, Phys. Rev. Lett. **80**, 956 (1998).
[11] Y. Wang, X. Hu, X. Xu, B. Cheng, and D. Zhang, Phys. Rev. B **68**, 165106 (2003).
[12] M. E. Zoorob, M. D. B. Charlton, G. J. Parker, J. J. Baumberg, and M. C. Netti, Nature (London) **404**, 740 (2000).
[13] S. David, A. Chelnokov, and J. M. Lourtioz, Opt. Lett. **25**, 1001 (2000).
[14] C. Jin, B. Cheng, B. Man, Z. Li, and D. Zhang, Phys. Rev. B **61**, 10762 (2000).
[15] M. A. Kaliteevski, S. Brand, R. A. Abram, T. F. Krauss, P. Millar, and R. M. De La Rue, J. Phys.: Condens. Matter **13**, 10459 (2001).
[16] K. Wang, S. David, A. Chelnokov, and J. M. Lourtioz, J. Mod. Opt. **50**, 2095 (2003).
[17] D. Sutter-Widmer, S. Deloudi, and W. Steurer, Phys. Rev. B **75**, 094304 (2007).
[18] K. Wang, Phys. Rev. B **76**, 085107 (2007).
[19] M. C. Rechtsman, H.-C. Jeong, P. M. Chaikin, S. Torquato, and

P. J. Steinhardt, Phys. Rev. Lett. **101**, 073902 (2008).
[20] K. Wang, Phys. Rev. B **73**, 235122 (2006).
[21] K. Mnaymneh and R. C. Gauthier, Opt. Express **15**, 5089 (2007).
[22] M. Bayindir, E. Cubukcu, I. Bulu, and E. Ozbay, Phys. Rev. B **63**, 161104(R) (2001).
[23] Y. Q. Wang, Z. F. Feng, X. S. Xu, B. Y. Cheng, and D. Z. Zhang, Europhys. Lett. **64**, 185 (2003).
[24] M. Notomi, H. Suzuki, T. Tamamura, and K. Edagawa, Phys. Rev. Lett. **92**, 123906 (2004).
[25] P.-T. Lee, T.-W. Lu, and F.-M. Tsai, IEEE Photon. Technol. Lett. **19**, 710 (2007).
[26] X. Xu, H. Chen, and D. Zhang, Appl. Phys. B **89**, 29 (2007).
[27] A. Micco, V. Galdi, F. Capolino, A. Della Villa, V. Pierro, S. Enoch, and G. Tayeb, Phys. Rev. B **79**, 075110 (2009).
[28] See R. G. Parr, *Quantum Theory of Molecular Electronic Structure* (Benjamin, New York, 1963), Chap. III.
[29] D. Gratias, A. Katz, and M. Quiquandon, J. Phys.: Condens. Matter **7**, 9101 (1995).
[30] H. Zhang and K. H. Kuo, Phys. Rev. B **42**, 8907 (1990).
[31] K. Wang and P. Garoche, Phys. Rev. B **55**, 250 (1997).
[32] See C. F. Bohren and D. R. Huffman, *Absorption and Scattering of Light by Small Particules* (Wiley, New York, 1983), Chaps. 3 and 8, Appendix C.
[33] M. V. Jarić and S. Y. Qiu, in *Quasicrystals: Proceedings of 12th Taniguchi Symposium*, edited by T. Fujiwara and T. Ogawa (Springer-Verlag, Berlin, 1990), p. 48.
[34] K. Edagawa, K. Suzuki, M. Ichihara, and S. Takeuchi, Philos. Mag. B **64**, 629 (1991).
[35] M. Duneau, R. Mosseri, and C. Oguey, J. Phys. A **22**, 4549 (1989).